Spatially Resolved Surface-Charge Measurement in a Planar Dielectric-Barrier Discharge System

L. Stollenwerk,* J. G. Laven, and H.-G. Purwins
Institut für Angewandte Physik, Corrensstraße 2/4, 48149 Münster, Germany
(Received 17 January 2007; published 18 June 2007)

We investigate a laterally extended dielectric helium discharge system with plane electrodes. The system is operated in the glow mode and is known to exhibit a rich variety of self-organized lateral patterns in the current distribution, most of them being filamentary. It is known from theory that surface charges on the dielectrics play a major role for the emerging patterns. In this work we present a method to measure the spatial charge distribution on the dielectrics via the Pockels effect of a bismuth-silicon-oxide crystal. The experimental results of the surface-charge distribution measurements are in good agreement with previous numerical solutions of the corresponding transport equations.

DOI: 10.1103/PhysRevLett.98.255001 PACS numbers: 52.80.−s, 51.50.+v, 89.75.Fb

Dielectric-barrier discharge (DBD) is a technique with a broad range of application, e.g., in the field of lighting, surface treatment, environmental protection, or plasma display panels [1,2]. Moreover, in recent research experimental systems with large lateral extensions and narrow discharge, gaps have been of increasing interest. Because of self-organization these systems tend to form a laterally structured discharge exhibiting a wide variety of patterns [3–7]. It has turned out that surface charges play an essential role in the process of generation and stabilization of the emerging patterns as the charges serve as memory between the breakdowns of consecutive half-cycles of the driving voltage [3,8]. Therefore, we are interested in a direct and spatially resolved measurement of the surface-charge distribution in a patterned DBD.

In recent works, the Pockels effect of different electro-optic crystals has been used to measure surface charges. Measurements of surface charges in scaled plasma display cells have been made by this technique [9,10]. The spatial resolution in [10] was achieved by scanning the discharge area with a laser beam. This method is rather time consuming and yields only modest resolution. A more convenient approach is presented in [11] and improved in [12,13], by which the whole discharge area can be recorded at once. However, in this case the experiment is run and afterwards the static pattern is recorded.

A sketch of our discharge cell is shown in Fig. 1. The $Bi_{12}SiO_{20}$ (BSO) crystal has a thickness of $a_{BSO} = 0.7$ mm. The gas gap is filled with helium at a pressure p in the range of 200 h Pa to 400 h Pa and has a width of $d = 0.8$ mm. The diameter D of the discharge area is 40 mm. The aluminum mirror is grounded and the system is driven with a positive rectangular voltage with a duty cycle of 50%, a frequency f of 14 kHz, and a pulse height U_{pp} in the range of 300 V to 500 V, which is fed to the contact spring. According to [14], at these conditions the discharge operates in glow mode, with one breakdown per half-cycle. The discharge cell is a modified version of the setup used in recent studies of pattern formation [6].

The optical setup is depicted in Fig. 2. The discharge cell is illuminated by a polarized light beam from a narrowband high flux 5 W light emitting diode (LED) emitting at 640 nm with a FWHM of 20 nm. The filter in front of camera 1 transmits only light from the narrowband high flux LED and blocks the entire spectrum of the He discharge. The $\lambda/8$-wave plate alters the working point of the polarizing optic to the maximum sensitivity for the electric field and makes the system sensitive to the sign of the surface charges.

Surface charges accumulating on the (001) face of the BSO crystal during breakdown cause the voltage U_{BSO} along the [001] direction of the BSO crystal which, in turn, induces a relative phase retardation among wave fronts of the incident light polarized along the fast and the slow axes of the BSO crystal via the electro-optic Pockels effect. The phase retardation is given by

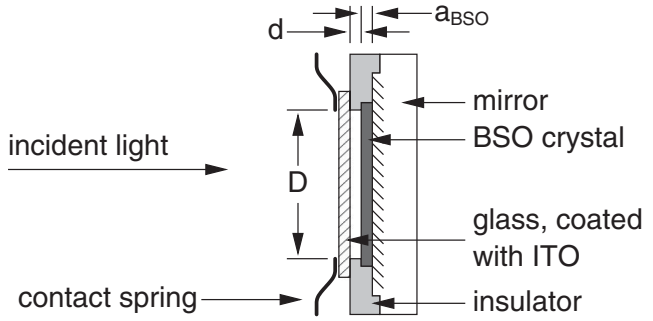

FIG. 1. Sketch of the discharge cell. The BSO crystal with thickness a_{BSO} is cemented to the reflecting surface of an Al mirror. Together with the BSO crystal, the mirror acts as a dielectrically coated electrode. The insulator defines the discharge gap length d and diverts mechanical stress caused by the contact springs away from the BSO crystal. A circular cutout in the insulator defines the discharge area with diameter D. The indium tin oxide (ITO) coated glass plate serves as second, transparent electrode.

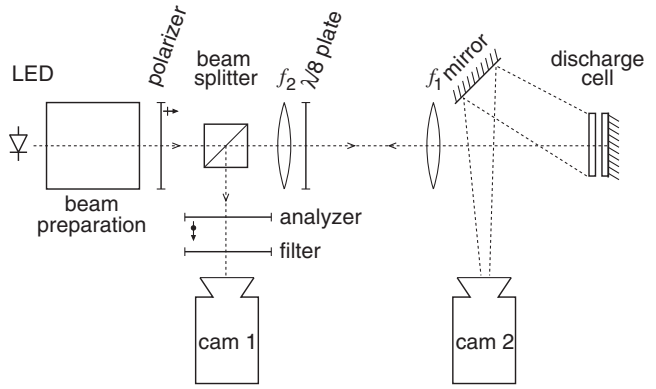

FIG. 2. Sketch of the optic setup. The light of the LED is prepared to be homogeneous and linearly polarized. The beam is expanded by f_1 and f_2 to illuminate the whole discharge cell. The reflected light is redirected to the analyzer, passes the bandpass filter, and reaches camera 1. Camera 2 observes the luminescence distribution in the discharge cell with help of a mirror.

$$\Delta\Phi = \frac{2\pi}{\lambda} n_0^3 r_{41} U_{\mathrm{BSO}} \quad \text{with} \quad U_{\mathrm{BSO}} = \frac{a_{\mathrm{BSO}}}{\varepsilon_0 \varepsilon_{\mathrm{BSO}}} \sigma, \tag{1}$$

where λ is the wavelength of the incident light, index $n_0 = 2.54$ the refraction, $r_{41} = 5$ pm/V electro-optical coefficient, and $\varepsilon_{\mathrm{BSO}} = 56$ the relative dielectric constant of BSO. The light intensity observed through the analyzer by camera 1 is

$$I = \frac{I_0}{2}\left[1 + \sin\left(2\frac{2\pi}{\lambda} n_0^3 r_{41} \frac{a_{\mathrm{BSO}}}{\varepsilon_0 \varepsilon_{\mathrm{BSO}}} \sigma\right)\right]. \tag{2}$$

I_0 is the LED light intensity. The additional phase retardation of the $\lambda/8$-wave plate shifts the working point of Eq. (2) into the linear regime. The expected surface-charge density in this system is in the order of a few nC/cm^2 according to recent numerical simulation [8] as well as experimental estimations done by separating the active current using a wheatstone bridge technique in the ac discharge. In this region the sinusoidal part of Eq. (2) can be linearized without experimentally noticeable error. The linearized equation for the light intensity at camera 1 is therefore

$$I = I_0\left(\frac{1}{2} + \frac{2\pi}{\lambda} n_0^3 r_{41} \frac{a_{\mathrm{BSO}}}{\varepsilon_0 \varepsilon_{\mathrm{BSO}}} \sigma\right). \tag{3}$$

As the optical system produces a spatially resolved picture $I(x, y)$ of the parallel light beam traversing the surface of the BSO crystal, Eq. (3) holds for every point on the BSO surface. To eliminate I_0 from Eq. (3), a reference image $I_r(x, y)$ with zero surface charge σ and a known voltage U^r_{BSO}, being a fraction of the driving voltage over the BSO crystal, is chosen. The spatially resolved surface-charge density distribution is then given by

$$\sigma(x, y) = \left[\frac{I(x, y)}{I_r(x, y)}(2kU^r_{\mathrm{BSO}} + 1) - 1\right]\frac{1}{2k}\frac{\varepsilon_0 \varepsilon_{\mathrm{BSO}}}{a_{\mathrm{BSO}}}$$
$$\text{with} \quad k = \frac{2\pi}{\lambda} n_0^3 r_{41}. \tag{4}$$

Hence, the spatially resolved surface-charge density $\sigma(x, y)$ can be obtained from the reference image $I_r(x, y)$ recorded without surface charges, and the measured image $I(x, y)$, recorded with surface charges while the discharge burns. Figure 3 gives an example of a pair of directly measured images $I_r(x, y)$ and $I(x, y)$.

As the time scales of the observed patterns in this system are often in the range of seconds, conventional video cameras with a frame rate of 25 fps are sufficient for observation of the luminescence density distribution (camera 2) and the phase retardation as a function of the surface-charge density distribution (camera 1). Each obtained camera frame comprises 280 driver periods. In order to observe the surface-charge distribution always with the same phase with respect to the driver, the LED is pulsed according to Fig. 4. The cell is illuminated during the positive half-cycles to measure positive surface charges and during the negative half-cycles to measure negative surface charges, respectively. To enhance the signal-to-noise ratio (SNR) it is taken advantage of the slow dynamic of the observed patterns in the system. It is often possible to increase the overall averaging time interval t_{av} by averaging over several 10 frames without losing lateral resolution in the region of interest.

The accuracy for a homogeneous charge density is limited by the camera accuracy and is 0.2 nC/cm^2; taking the camera noise and the above averaging processes into account, the final accuracy is of the order of 0.5 nC/cm^2. The spatial resolution corresponds to the thickness of the BSO crystal and is 0.7 mm. From this we conclude that the minimum detectical charge from the area of 0.7 mm $\times$ 0.7 mm is 2.5 pC.

The final results of our measurements are presented in Fig. 5. On the left-hand side the luminescence density distribution in the discharge observed by camera 2 is shown. On the right-hand side the corresponding surface-charge density distribution is displayed. Since the picture taken by camera 2 has been transformed onto the coordi-

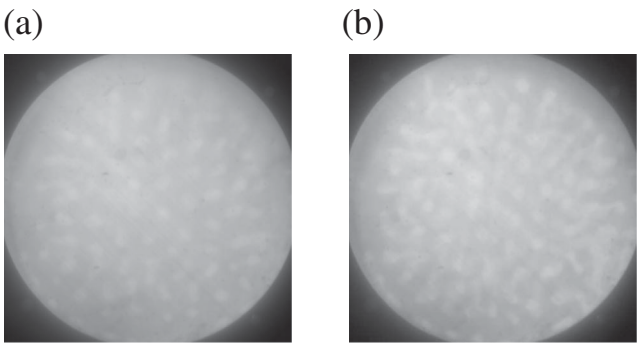

FIG. 3. (a) Reference image $I_r(x, y)$ from camera 1 taken before the discharge. (b) Raw image $I(x, y)$ from camera 1 while the discharge burns, averaged over 22 video frames. The visible structures are discolorations of the BSO crystal. The charges become visible after calculating σ according to Eq. (4). The result is shown in Fig. 5(a).

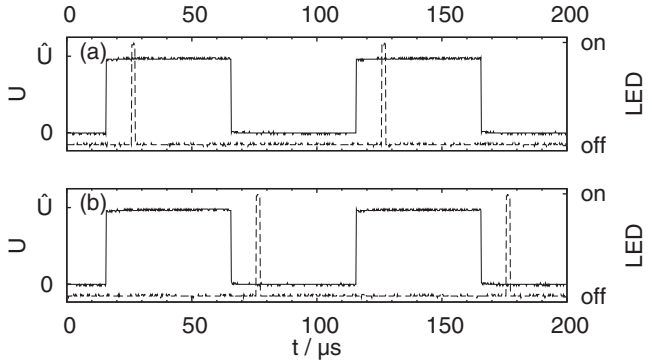

FIG. 4. Timing of the LED pulses (dashed line) relative to the driving voltage (solid line). (a) Illumination in the positive half-cycle; (b) illumination in the negative half-cycle.

nate system of camera 1, pixels in both pictures represent densities at the same lateral position in the discharge cell. Because of the different sign of phase retardation $\Delta\Phi$ corresponding to the sign of the surface charge σ positive surface charges appear as bright spots, while negative surface charges appear dark. In Fig. 5(a) a structured DBD with a few high current filaments on a low current background is investigated. The surface-charge distribution is taken during the positive half-cycle of the driver voltage. At positions occupied with high current filaments, i.e., bright spots in the luminescence radiation density, areas with high positive surface-charge densities can be seen. Because of some dynamics of the discharge pattern some filaments have moved during averaging and appear blurred.

In Fig. 5(b) a similar measurement at the negative half-cycle of the driver voltage has been made. The DBD system again exhibits a few high current filaments in front of a low current background. In contrast to the previous measurement, these time surface charges with negative sign are observed.

Figures 5(c) and 5(d) are taken at a relatively high driving voltage U_{pp} and rather high helium pressure p. At these parameters a transition to a dense filamentary discharge has taken place. The surface-charge densities in Fig. 5(c) and 5(d) are taken during the positive and the negative half-cycle of the driver voltage, respectively. Again, the surface-charge density is an image of the current density (observed via the luminescence radiation), and the sign of the surface charges corresponds to the half-cycle of the driver voltage.

The rectangular driver voltage between 0 V and U_{pp} can be considered as a dc voltage of $U_{pp}/2$ superposed by a rectangular ac voltage with an amplitude of $U_{pp}/2$. As a result, the electric potential of the discharge cell is shifted by this offset voltage $U_{pp}/2$ relative to ground potential. As the electrode to which the BSO crystal is cemented is grounded, the potential difference across the crystal causes an offset in the phase retardation, i.e., surface-charge density. This offset can be seen in the measured surface-

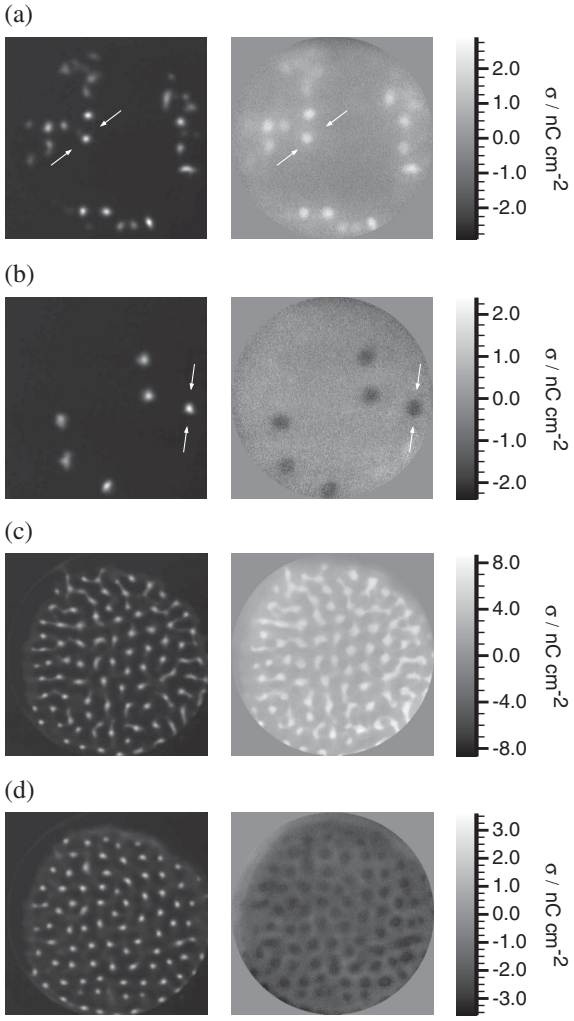

FIG. 5. Luminescence radiation density of the discharge area (left) and corresponding surface-charge density (right). Parameters: (a) $U_{pp} = 330$ V, $p = 260$ h Pa, $t_{av} = 880$ ms, positive half-cycle; (b) $U_{pp} = 330$ V, $p = 260$ h Pa, $t_{av} = 440$ ms, negative half-cycle; (c) $U_{pp} = 400$ V, $p = 345$ h Pa, $t_{av} = 3$ s, positive half-cycle; (d) $U_{pp} = 400$ V, $p = 330$ h Pa, $t_{av} = 2.7$ s, negative half-cycle. The arrows depict the charge spots to which Fig. 6 refers.

charge densities in Fig. 5. In Figs. 5(a) and 5(b) taken at $U_{pp} = 330$ V the surface-charge densities are up to $\sigma = 2.9$ nC/cm^2 for the positive species and $\sigma = -2.4$ nC/cm^2 for the negative species. At a driver voltage pulse height of $U_{pp} = 400$ V the surface-charge densities are found to be $\sigma = 8.7$ nC/cm^2 for the positive and $\sigma = -3.6$ nC/cm^2 for the negative species, respectively.

In Fig. 6 the radial luminescence distribution as well as the radial surface-charge distribution for two filaments is shown. The Gaussian function

$$f(x) = \frac{A}{2\pi\delta^2}\exp\left(-\frac{x^2}{2\delta^2}\right) + b \qquad (5)$$

is fitted to all distributions to determine the width ($2\delta_\sigma$,

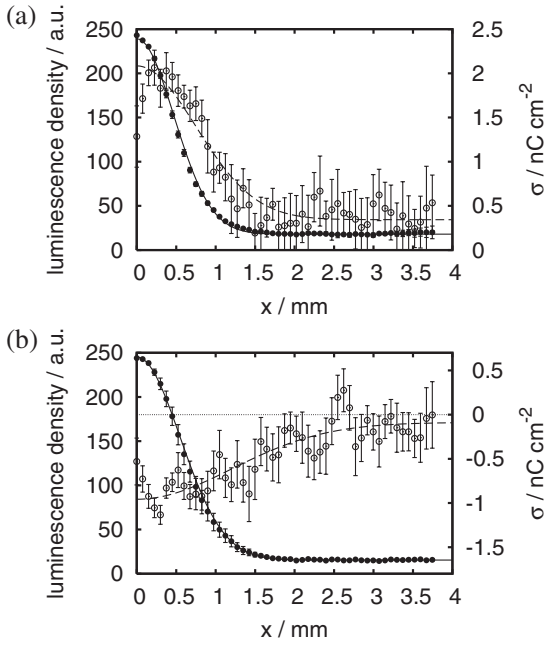

FIG. 6. Azimuthally averaged luminescence density ● and surface charge distribution ○ at the position of a filament in the (a) positive and (b) negative half-cycle of the driver voltage. The error bars correspond to the standard deviation from the azimuthal averaging. The graphs (a) and (b) correspond to the marked filaments in Fig. 5(a) and 5(b). Filament properties according to Eq. (5): (a) $\delta_\sigma = 0.75$ mm, $\delta_{\text{lum}} = 0.47$ mm, $A_\sigma = 61$ pC, $A_{\text{lum}} = 307$ a.u.; (b) $\delta_\sigma = 1.20$ mm, $\delta_{\text{lum}} = 0.55$ mm, $A_\sigma = -79$ pC, $A_{\text{lum}} = 405$ a.u..

$2\delta_{\text{lum}}$) and the overall charge (A_σ) or integral brightness (A_{lum}) of the filament. The negative surface charges are significantly broader than the distribution of the luminescence density. The positive surface charges are broader than the luminescence density, too, but this is at least partly due to the spatial resolution of the measurement limited by the BSO crystal thickness. Evaluations of further filaments lead to a ratio of surface-charge width to luminescence density width $\delta_\sigma/\delta_{\text{lum}}$ of 1.4 to 2.0 for positive charges and 2.1 to 3.0 for negative surface charges. Hence, the negative surface-charge distribution of a filament is broader than the positive one, and the latter is at least as broad as the luminescence radiation density. This poses as an explanation for the interaction law of filaments previously inaccessible by the mere observation of the luminescence distribution. First of all, for dense filaments, as seen in Fig. 5(d), the distance between filaments is much larger than the filament diameter in the luminescence radiation but it is almost the same as that of the negative surface charges. Essentially the same is true for interacting filaments, as observed in [15,16]: the distance, at which annihilation is observed, is also of the order of the negative surface-charge distribution.

It is known from earlier investigations [15] that the integral brightness of the whole domain is proportional to the transferred charge. It is interesting to note that in the present Letter we demonstrate for the first time that this is also true for individual filaments. The proportionality of integral brightness and transferred charge within a filament allows for relative charge and current density estimations in patterns comprising filaments with different brightness, as observed, e.g., in [15].

We remark further that in [8] it was possible to calculate quantitatively the amount of surface charges. In these calculations one finds a peak surface-charge density of 7 nC/cm^2 which is well within the experimental results of 6 nC/cm^2 $\pm 50\%$ predented here. Last but not least, the above-mentioned difference in the extension of the measured positive and negative surface charge is in good agreement with recently obtained results in the numerical simulation of single filaments [17].

Finally we stress that the accuracy and time resolution can definitely be improved by using a camera with larger dynamics and repetition rate. This might make it possible to observe the temporal behavior of the surface charges within a single breakdown.

This work was supported by the Deutsche Forschungsgemeinschaft (DFG).

*stollenw@uni-muenster.de

[1] J. P. Boeuf, J. Phys. D: Appl. Phys. **36**, R53 (2003).
[2] U. Kogelschatz, Plasma Chem. Plasma Process. **23**, 1 (2003).
[3] W. Breazeal, K. M. Flynn, and E. G. Gwinn, Phys. Rev. E **52**, 1503 (1995).
[4] E. L. Gurevich, A. L. Zanin, A. S. Moskalenko, and H.-G. Purwins, Phys. Rev. Lett. **91**, 154501 (2003).
[5] L. Stollenwerk, S. Amiranashvili, and H.-G. Purwins, New J. Phys. **8**, 217 (2006).
[6] L. Stollenwerk, S. Gurevich, J. G. Laven, and H.-G. Purwins, Eur. Phys. J. D **42**, 273 (2007).
[7] L. Dong, F. Liu, S. Liu, Y. He, and W. Fan, Phys. Rev. E **72**, 046215 (2005).
[8] L. Stollenwerk, S. Amiranashvili, J.-P. Boeuf, and H.-G. Purwins, Phys. Rev. Lett. **96**, 255001 (2006).
[9] K. Sugimoto, H. Takahashi, O. Shimomura, and T. Sakurai, J. Phys. D: Appl. Phys. **36**, 2887 (2003).
[10] D. C. Jeong, H. S. Bae, and K. W. Whang, J. Appl. Phys. **97**, 013304 (2005).
[11] T. Kawasaki, T. Terashima, S. Suzuki, and T. Takada, J. Appl. Phys. **76**, 3724 (1994).
[12] T. Kawasaki, T. Terashima, Y. Zhu, T. Takada, and T. Maeno, J. Phys. D: Appl. Phys. **27**, 1646 (1994).
[13] Y. Zhu, T. Takada, and T. Demin, J. Phys. D: Appl. Phys. **28**, 1468 (1995).
[14] I. Radu, R. Bartnikas, and M. R. Wertheimer, J. Appl. Phys. **95**, 5994 (2004).
[15] I. Brauer, Ph.D. thesis, Westfälische Wilhelms-Universität Münster, 2000.
[16] I. Müller, E. Ammelt, and H.-G. Purwins, in *International Conference on Phenomena in Ionized Gases ICPIG XXIII* (CPAT, Toulouse, 1997), Vol. II-182–II-183.
[17] L. Stollenwerk, S. Amiranashvili, J.-P. Boeuf, and H.-G. Purwins, Eur. Phys. J. D (to be published).